Confinement and the photon propagator in 3D compact QED: A lattice study in the Landau gauge at zero and finite temperature

M. N. Chernodub
Institute of Theoretical and Experimental Physics, B. Cheremushkinskaja 25, Moscow, 117259, Russia
and Institute for Theoretical Physics, Kanazawa University, Kanazawa 920-1192, Japan

E.-M. Ilgenfritz
Research Center for Nuclear Physics, Osaka University, Osaka 567-0047, Japan

A. Schiller
Institut für Theoretische Physik and NTZ, Universität Leipzig, D-04109 Leipzig, Germany
(Received 22 August 2002; published 13 February 2003)

On the lattice we study the gauge boson propagator of three-dimensional compact QED in the Landau gauge at zero and nonzero temperature. The nonperturbative effects are taken into account by the generation of a mass, by an anomalous dimension, and by photon wave function renormalization. All these effects can be attributed to the monopoles: they are absent in the propagator of the singularity-free part of the gauge field. We assess carefully the Gribov copy problem for the propagator and the parameters emerging from the fits.

DOI: 10.1103/PhysRevD.67.034502 PACS number(s): 11.15.Ha, 11.10.Wx, 12.38.Gc

I. INTRODUCTION

Three-dimensional compact electrodynamics ($cQED_3$) has two essential features in common with QCD: confinement [1] and chiral symmetry breaking [2]. Although the physics behind it might be very different, monopole dynamics in three and in four dimensions, it is amusing to study certain nonperturbative aspects within a lower-dimensional model such as $cQED_3$. Apart from its role as a toy model for QCD, the nonperturbative properties of $cQED_3$ deserve attention in themselves because this model was shown to describe some features of Josephson junctions [3] and high-T_c superconductors [4]. $cQED_3$ was the first example, in space-time dimensions greater than two where it becomes a nontrivial problem, in which confinement of electrically charged particles was understood analytically [1]. It is the result of the dynamics of monopoles which emerge due to the compactness of the gauge field. Other common features of $cQED_3$ and QCD are the existence of a mass gap and of a confinement-deconfinement phase transition at some nonzero temperature.

In two recent papers we demonstrated how the deconfinement phase transition, occurring under the influence of compactification of one dimension, in $2+1$ dimensions, finds its explanation from the monopole point of view [5] and why the deconfinement phase transition is independent of the strength of the external fields [6].

In a recent Letter [7] we answered the question of what effect the confinement property has on the gauge boson propagator in this theory and what part of the propagator is changing at the deconfinement temperature. The effects are twofold: First, an anomalous dimension appears which modifies the momentum dependence, and second, a mass is generated which can be well understood in terms of Polyakov's theory [1]. In Ref. [7] we also used the unique possibility in lattice simulations to remove the monopole degrees of freedom from the quantum gauge field in order to show that all nontrivial effects reside exclusively in the singular fields of the monopoles.

Note that a nontrivial anomalous dimension of the gauge boson propagator may also appear due to dynamical matter fields [8]. The sign (in our notation) of the anomalous dimension induced in this way is different, and this leads to the binding of the monopoles into dipole pairs and, consequently, to the disappearance of the confinement at certain distances between the test particles. This picture was confirmed for a compact model in the presence of dynamical matter fields [9].

In the present paper we want to extend the analysis of Ref. [7] in various respects. Since the propagator is studied in the Landau gauge, first of all we have investigated more carefully the quality of the gauge fixing and the importance of the Gribov copy problem, first on the propagator itself and then on the parameters that finally describe the functional form of the propagator.

In a second direction, we investigate the potential influence that different definitions of the gauge potential A_μ in terms of the lattice link fields might have on the resulting propagator. One of the choices is strongly recommended by the explicit gauge invariance (transversality) of the emerging propagator. However, in the case when the longitudinal part does not vanish by construction, proper selection of the transversal component also leads to almost the same fit parameters. The coincidence becomes obviously better at larger β.

Going over from zero to finite temperature, it is important to realize that more structure functions are necessary to describe the finite-temperature case. One of them, the deconfinement-sensitive D_L, has been studied already in Ref. [7], while the other, D_T, has been found to be extremely sensitive to the Gribov problem. Only by exerting extreme care can one expose the change going on at the deconfinement transition.

The paper is organized as follows. In Sec. II we define the lattice model and the tensorial structure of the propagators, at $T=0$ and for $T\neq 0$. Section III contains a discussion of the minimal Landau gauge which points out the topological aspects related to the gauge fixing, in particular the condition of having a minimal total length of Dirac strings. In Sec. IV we report on the numerical algorithms for updating and gauge fixing that we have used in our investigation. The following Sec. V is devoted to an outline of the results for $T=0$. Section VI describes the particular requirements of gauge fixing in the $T\neq 0$ case and contains our results for the propagators D_L and D_T. Some conclusions are formulated in Sec. VII.

II. THE 3D COMPACT U(1) MODEL AND THE PHOTON PROPAGATOR

For the compact U(1) model we chose the Wilson single-plaquette action:

$$S[\theta_l]=\beta\sum_p (1-\cos\theta_p), \tag{1}$$

where θ_p is the U(1) field strength tensor represented by the plaquette curl of the compact link field θ_l. The lattice is three dimensional, and the basic degrees of freedom are the links $U_l=\exp(i\theta_l)$. The measure of the link angles is flat over the interval $-\pi<\theta\leqslant\pi$. The lattice coupling constant β is related to the lattice spacing a and the continuum coupling constant g_3 of the 3D theory,

$$\beta=1/(ag_3^2). \tag{2}$$

Note that in three-dimensional gauge theory the coupling constant g_3 has dimension $(\text{mass})^{1/2}$. Zero physical temperature is represented by symmetric lattices, $L_t=L_s$.[1] The lattice corresponding to finite temperature is asymmetric, $L_s^2\times L_t$, $L_t\ll L_s$. In the limit $L_s\to\infty$, the temporal extension of the lattice is related to the physical temperature, $L_t=1/(Ta)$. Using Eq. (2) the temperature is given in units of g_3^2 in terms of the lattice parameters as follows:

$$\frac{T}{g_3^2}=\frac{\beta}{L_t}. \tag{3}$$

Our simulations for zero temperature have been performed mainly on a 32^3 lattice, those at finite temperature on a $32^2\times 8$ lattice.

The final discussion of the photon propagator will be given in lattice momentum space. Being always defined in a specified gauge, the propagator is written in terms of the Fourier transformed gauge potential,

$$\tilde{A}_{\vec{k},\mu}=\frac{1}{\sqrt{L_1L_2L_3}}\sum_{\vec{n}}\exp\left(2\pi i\sum_{\nu=1}^{3}\frac{k_\nu\left(n_\nu+\frac{1}{2}\delta_{\nu\mu}\right)}{L_\nu}\right)A_{\vec{n}+(1/2)\vec{\mu},\mu}, \tag{4}$$

which is a sum over a certain discrete set of points $\vec{x}=\vec{n}+\frac{1}{2}\vec{\mu}$ forming the support of $A_{\vec{x},\mu}$ on the lattice. These are the midpoints of the links in the μ direction while $\vec{n}$ denotes the lattice sites (nodes) with integer Cartesian coordinates. The propagator is the gauge-fixed ensemble average of the following bilinear in $\tilde{A}$:

$$D_{\mu\nu}(\vec{p})=\langle\tilde{A}_{\vec{k},\mu}\tilde{A}_{-\vec{k},\nu}\rangle. \tag{5}$$

Two identifications of $A_{\vec{x},\mu}$ have been adopted in the literature and will be compared in our paper: the *angle* definition

$$A_{\vec{n}+(1/2)\vec{\mu},\mu}=\theta_{\vec{n},\mu}/(g_3a)=\log(U_{\vec{n},\mu})/(ig_3a) \tag{6}$$

and the sine definition

$$A_{\vec{n}+(1/2)\vec{\mu},\mu}=\sin(\theta_{\vec{n},\mu})/(g_3a)=(U_{\vec{n},\mu}-U^*_{\vec{n},\mu})/(2ig_3a). \tag{7}$$

The corresponding propagators will be denoted as $D^{ang}_{\mu\nu}$ and $D^{sin}_{\mu\nu}$, respectively.

The lattice momenta $\vec{p}$ on the left hand side of Eq. (5) are related to the integer valued Fourier momenta $\vec{k}$ as follows:

$$p_\mu(k_\mu)=\frac{2}{a}\sin\frac{\pi k_\mu}{L_\mu},\quad k_\mu=0,\pm 1,\ldots,\pm\frac{L_\mu}{2}. \tag{8}$$

The lattice equivalent of $p^2=\vec{p}^2$ is in 3D

$$p^2(\vec{k})=\frac{4}{a^2}\sum_{\mu=1}^{3}\left(\sin\frac{\pi k_\mu}{L_\mu}\right)^2. \tag{9}$$

At zero temperature, based on Euclidean rotational invariance, the continuum propagator would be expressible by functions of p^2. The most general tensor structure is then the following one including two scalar functions of p^2:

$$D_{\mu\nu}(\vec{p})=P_{\mu\nu}(\vec{p})D(p^2)+\frac{p_\mu p_\nu}{p^2}\frac{F(p^2)}{p^2} \tag{10}$$

with the d-dimensional (in our case $d=3$) transverse projection operator

$$P_{\mu\nu}(\vec{p})=\delta_{\mu\nu}-\frac{p_\mu p_\nu}{p^2}. \tag{11}$$

The projector has the properties

[1] L_t is the extension in the third (z) direction.

$$P_{\mu\alpha}(\vec{p})P_{\alpha\nu}(\vec{p})=P_{\mu\nu}(\vec{p}),\quad P_{\mu\mu}(\vec{p})=d-1. \tag{12}$$

The two structure functions $D(p^2)$ and $F(p^2)$ can be extracted by projection on the lattice from $D_{\mu\nu}(\vec{p})$ according to Eq. (5), as

$$F(p^2)=\sum_{\mu,\nu=1}^{3} p_\mu D_{\mu\nu}(\vec{p})p_\nu \tag{13}$$

and

$$p^2D(p^2)=\frac{1}{d-1}P_{\mu\nu}(\vec{p})D_{\mu\nu}(\vec{p}). \tag{14}$$

They are found to be, in the best case, only approximately rotationally invariant, i.e., individual momenta $\vec{p}$ might slightly differ in the function values D or F they provide, even if they have the same p^2. Dense data points close together in p^2 might scatter rather than forming a smooth function of p^2.

In practice, using these definitions, we extract first the function $F(p^2)$ in the $d=3$ case through

$$\begin{aligned}F(p^2)=&p_1^2D_{11}(\vec{p})+p_2^2D_{22}(\vec{p})+p_3^2D_{33}(\vec{p})\\&+2p_1p_2\ \mathrm{Re}\ D_{12}(\vec{p})+2p_1p_3\ \mathrm{Re}\ D_{13}(\vec{p})\\&+2p_2p_3\ \mathrm{Re}\ D_{23}(\vec{p}).\end{aligned} \tag{15}$$

The imaginary parts of nondiagonal $D_{\mu\nu}$ cancel in the sum and have been omitted. Then the function $D(p^2)$ is obtained through

$$D(p^2)=\frac{1}{d-1}\{[D_{11}(\vec{p})+D_{22}(\vec{p})+D_{33}(\vec{p})]-F(p^2)/p^2\}. \tag{16}$$

If the Landau gauge were exactly fulfilled, one would expect that $F(p^2)\equiv 0$. On the lattice, in the case of the sine definition for $A_{x,\mu}$, this is actually the case as soon as one of the Gribov copies is reached, with an accuracy that directly reflects the stopping precision of the gauge-fixing procedure (as will be discussed below). In this case, a simplified definition in terms of the diagonal components $D_{\mu\mu}(\vec{p})$ would be appropriate. In case of the angle definition the structure function $F(p^2)$ does not vanish; therefore all components of $D_{\mu\nu}(\vec{p})$ contribute to $D(p^2)$.

For the finite-temperature case, the propagator lacks $O(3)$ rotational symmetry. Now we have to consider two scalar functions D_T and D_L instead of D, multiplying the $(d-1)$-dimensional transverse projection operator P^T and the $(d-1)$-dimensional longitudinal projection operator P^L, respectively. The scalar functions D_T, D_L, and F depend now separately on the length of the spacelike part of $\vec{p}$ with $i=1,\ldots,d-1$,

$$\mathbf{p}^2=p_1^2+\cdots+p_{d-1}^2,\quad |\mathbf{p}|=\sqrt{\mathbf{p}^2}, \tag{17}$$

and the "temporal" momentum p_d,

$$\begin{aligned}D_{\mu\nu}(\vec{p})=&P^T_{\mu\nu}(\vec{p})D_T(|\mathbf{p}|,p_d)+P^L_{\mu\nu}(\vec{p})D_L(|\mathbf{p}|,p_d)\\&+\frac{p_\mu p_\nu}{p^2}\frac{F(|\mathbf{p}|,p_d)}{p^2}.\end{aligned} \tag{18}$$

The two projection operators are defined as follows $(i,j=1,\ldots,d-1)$: a transverse one,

$$P^T_{ij}(\vec{p})=\delta_{ij}-\frac{p_ip_j}{\mathbf{p}^2},$$

$$P^T_{dd}(\vec{p})=P^T_{di}(\vec{p})=P^T_{id}(\vec{p})=0, \tag{19}$$

and a longitudinal one

$$P^L_{\mu\nu}(\vec{p})=P_{\mu\nu}(\vec{p})-P^T_{\mu\nu}(\vec{p}). \tag{20}$$

Obviously, these projectors have the properties

$$P^T_{\mu\alpha}(\vec{p})P^T_{\alpha\nu}(\vec{p})=P^T_{\mu\nu}(\vec{p}),\quad P^T_{\mu\mu}(\vec{p})=d-2, \tag{21}$$

$$P^L_{\mu\alpha}(\vec{p})P^L_{\alpha\nu}(\vec{p})=P^L_{\mu\nu}(\vec{p}),\quad P^L_{\mu\mu}(\vec{p})=1, \tag{22}$$

$$P^L_{\mu\alpha}(\vec{p})P^T_{\alpha\nu}(\vec{p})=0. \tag{23}$$

The scalar functions D_T and D_L can be extracted from $D_{\mu\nu}(\vec{p})$ via

$$P^T_{\mu\nu}(\vec{p})D_{\mu\nu}(\vec{p})=(d-2)D_T(|\mathbf{p}|,p_d), \tag{24}$$

$$\begin{aligned}P^L_{\mu\nu}(\vec{p})D_{\mu\nu}(\vec{p})=&D_L(|\mathbf{p}|,p_d)\\=&(d-1)D(|\mathbf{p}|,p_d)-(d-2)D_T(|\mathbf{p}|,p_d).\end{aligned} \tag{25}$$

For $d=3$ we can write down explicitly the definitions

$$\mathbf{p}^2D_T(|\mathbf{p}|,p_d)=p_2^2D_{11}(\vec{p})+p_1^2D_{22}(\vec{p})-2p_1p_2\ \mathrm{Re}\ D_{12}(\vec{p}) \tag{26}$$

and

$$\begin{aligned}\mathbf{p}^2(\mathbf{p}^2+p_3^2)D_L(|\mathbf{p}|,p_d)=&\mathbf{p}^2[\mathbf{p}^2D_{33}(\vec{p})-2p_1p_3\ \mathrm{Re}\ D_{13}(\vec{p})\\&-2p_2p_3\ \mathrm{Re}\ D_{23}(\vec{p})]\\&+p_3^2[p_1^2D_{11}(\vec{p})+p_2^2D_{22}(\vec{p})\\&+2p_1p_2\ \mathrm{Re}\ D_{12}(\vec{p})].\end{aligned} \tag{27}$$

In the static limit, $p_3=0$,

$$D_L(|\mathbf{p}|,p_3=0)\equiv D_{33}(|\mathbf{p}|,p_3=0). \tag{28}$$

This propagator for the case of the angle definition and its fit in terms of mass and anomalous dimension as well as the changes at the deconfinement transition were discussed in Ref. [7].

In the case of $T=0$, the data to be presented below will be averaged over measurements of these quantities obtained for different $\vec{k}=(k_1,k_2,k_3)$ giving rise to the same p^2 according to Eq. (9). In the case $T\neq 0$ we will show data averaged over different (k_1,k_2) giving rise to the same $\mathbf{p}^2$ according to Eq. (17). One should keep in mind that by this "trick" one enforces the rotational invariance "by hand," and the statistical errors are reduced as compared to measurements for individual $\vec{k}$-components of the propagator.

In order to discuss the functional form of the propagator from the viewpoint of confinement effects, with the confinement being induced by the monopole plasma, we will decompose the gauge fields into singular (monopole) and regular (photon) contributions at the level of the link angles,

$$\theta_{\vec{n},\mu}=\theta^{phot}_{\vec{n},\mu}+\theta^{mono}_{\vec{n},\mu}, \tag{29}$$

by a procedure to be described below. After the decomposition (29) of the link angles is done, one may define the corresponding $A^{phot}_{\vec{n}+(1/2)\vec{\mu},\mu}$ and $A^{mono}_{\vec{n}+(1/2)\vec{\mu},\mu}$ through the angle definition (6) and the sine definition (7), respectively. Then, by fast Fourier transform, the corresponding $\tilde{A}^{phot}_{\vec{k},\mu}$ and $\tilde{A}^{mono}_{\vec{k},\mu}$ are evaluated. For each configuration and a certain set of momenta the bilinears for the photon part $\tilde{A}^{phot}_{\vec{k},\mu}\tilde{A}^{phot}_{-\vec{k},\nu}$ and the monopole part $\tilde{A}^{mono}_{\vec{k},\mu}\tilde{A}^{mono}_{-\vec{k},\nu}$ and the mixed bilinear $\tilde{A}^{phot}_{\vec{k},\mu}\tilde{A}^{mono}_{-\vec{k},\nu}$ are formed. These are the observables that are associated—by averaging over the Monte Carlo ensemble—with the propagators $D^{phot}_{\mu\nu}(\vec{p})$ (the photon or *regular* propagator), $D^{mono}_{\mu\nu}(\vec{p})$ (the *singular* propagator), and $D^{mixed}_{\mu\nu}(\vec{p})$ (the *mixed* propagator). These propagators are considered together with the *full* propagator, which uses the original link angles $\theta_{\vec{n},\mu}$ before the splitting (29) has been performed.

In the $T=0$ case, all these functions of $\vec{p}$ are then mapped by the projections (15),(16) to the scalar structure functions $D^{phot}(p^2)$, $D^{mono}(p^2)$, $D^{mixed}(p^2)$ and $F^{phot}(p^2)$, $F^{mono}(p^2)$, $F^{mixed}(p^2)$. In the finite-temperature case we proceed analogously.

For the angle definition of the vector potential we stress that the structure functions obviously satisfy exact additivity:

$$D(\vec{p})=D^{phot}(\vec{p})+D^{mono}(\vec{p})+2D^{mixed}(\vec{p}), \tag{30}$$

$$F(\vec{p})=F^{phot}(\vec{p})+F^{mono}(\vec{p})+2F^{mixed}(\vec{p}). \tag{31}$$

III. MONOPOLES, DIRAC STRINGS, AND THE MINIMAL LANDAU GAUGE

In this section we partially follow Ref. [10]. Gauge fixing to the Landau gauge means, for a given configuration $\theta_l=\theta_{\vec{n},\mu}$, finding gauge transformations $\omega_{\vec{n}}$ such that, for a *gauge functional*

$$\mathcal{F}(\theta)=\sum_l \cos(\theta_l), \tag{32}$$

the transformed gauge functional becomes maximal,

$$\max_\omega \mathcal{G}(\theta,\omega), \quad \mathcal{G}(\theta,\omega)=\mathcal{F}(\theta^{(\omega)}). \tag{33}$$

Here $\theta^{(\omega)}_l$ denotes the gauge transformed gauge field[2]

$$\theta\to\theta^{(\omega)}=\theta+d\omega_{2\pi}\equiv\theta+d\omega+2\pi k, \quad k\in\mathbb{Z}, \tag{34}$$

where the integer number $k=k(\theta,\omega)$ for each link is chosen such that $\theta^{(\omega)}\in(-\pi,\pi]$.

Instead of Eq. (33), following Ref. [10] we use for the purpose of this section the Villain form of the gauge condition,

$$\min_\omega ||\theta^{(\omega)}||^2. \tag{35}$$

The Faddeev-Popov (FP) determinant is introduced by the following decomposition of unity:

$$1=\Delta_{FP}[\theta;\lambda]\int_{-\pi}^{\pi}\mathcal{D}\omega e^{-\lambda||\theta^{(\omega)}||^2}, \tag{36}$$

where λ is the gauge-fixing parameter. In order to achieve the gauge (35) we have to send λ to infinity. In this case the limits of integration in Eq. (36) can be extended to $\pm\infty$ since the saddle point approximation is exact in the limit $\lambda\to\infty$. Moreover, the integer valued variable k in Eq. (34) becomes effectively independent of θ and ω since the values of k for which $\theta^{(\omega)}\notin(-\pi,\pi]$ are exponentially suppressed. Therefore, in the limit of infinite λ, the FP determinant (36) can be written as follows:

$$\Delta^{-1}_{FP}[\theta;\lambda]=\int_{-\infty}^{\infty}\mathcal{D}\omega\sum_{k\in\mathbb{Z}(c_1)}\exp\{-\lambda||\theta+d\omega+2\pi k||^2\}. \tag{37}$$

Using the Hodge–de Rahm transformation $k=\delta\Delta^{-1}dk+d\Delta^{-1}\delta k$, and making the shift $\omega\to\omega-\Delta^{-1}\delta k$, we get

$$\Delta^{-1}_{FP}[\theta;\lambda]=\text{const}\int_{-\infty}^{\infty}\mathcal{D}\omega \times\sum_{\substack{s\in\mathbb{Z}(c_2)\\ ds=0}}\exp\{-\lambda||\theta+d\omega+2\pi\delta\Delta^{-1}s||^2\}, \tag{38}$$

[2]Here and in the following we use the differential form notation on the lattice: $(a,b)=\Sigma_l a_l b_l$, $||\theta||^2=(\theta,\theta)$. The operations $d\theta$ and $\delta\theta$ are the lattice curl and divergence, respectively. The Laplacian is denoted as $\Delta=\delta d+d\delta$.

where we have changed the variables, $s=dk$. The integration over ω gives

$$\Delta_{FP}^{-1}[\theta;\lambda]=\text{const}\sum_{\substack{s\in Z(c_2)\\ ds=0}}\exp\{-\lambda(d\theta+2\pi\delta\Delta^{-1}s,\Delta^{-1}\times(d\theta+2\pi\delta\Delta^{-1}s)\}. \tag{39}$$

To proceed further we separate the gauge field θ into regular (photon) and singular (monopole) parts following Ref. [11]:

$$\theta=\theta^{phot}+\theta^{mono},\quad \theta^{mono}=2\pi\Delta^{-1}\delta p[j], \tag{40}$$

where the dual one-form $^*j$ represents the monopoles on the dual lattice sites. The one-form on the dual lattice, $p[j]$, defines the Dirac lines that connect the monopoles and antimonopoles, $\delta\,{}^*p[j]={}^*j$.

The photon part θ^{phot} is free of singularities while the monopole part θ^{mono} contains the information about all monopole singularities:

$$\frac{1}{2\pi}d[d\theta^{phot}]_{2\pi}=0,\quad \frac{1}{2\pi}d[d\theta^{mono}]_{2\pi}=j. \tag{41}$$

Here the DeGrand-Toussaint definition of the monopole [12] has been used. Substituting Eq. (40) into Eq. (39), we get, after a little algebra,

$$\Delta_{FP}^{-1}[\theta;\lambda]=\text{const}\times\exp\{4\lambda(j,\Delta^{-2}j)\}\times\sum_{\substack{s\in Z(c_2)\\ ds=0}}\exp\{-\lambda S_{gf}(\theta^{phot},p[j]+s)\}, \tag{42}$$

with

$$S_{gf}(\theta^{phot},p)=(d\theta^{phot}+2\pi p,\Delta^{-1}\{d\theta^{phot}+2\pi(p[j]+s)\}). \tag{43}$$

The meaning of the last equations is the following. The gauge transformation (34) contains both regular ($d\omega$) and singular (k) parts. The former transforms the photon part of the gauge field while the latter changes the monopole part, shifting the Dirac string (but leaving the monopoles j intact). We have already integrated out the regular gauge transformations; therefore Eq. (42) depends explicitly on $d\theta^{phot}$ which is invariant under regular gauge transformations $\theta^{phot}\to\theta^{phot}+d\omega$. The sum in Eq. (42) over all possible shifts of the Dirac lines,

$$^*p[j]\to{}^*p[j]+{}^*s, \tag{44}$$

corresponds to integration over all singular gauge transformations (remember that $^*s$ is the closed line on the dual lattice, $\delta\,{}^*s=0$). Thus Eq. (42) is implicitly invariant under the singular gauge transformations as well.

In the limit $\lambda\to\infty$ the only contribution to the FP determinant is given by the *global* minimum of the gauge-fixing functional (43) with respect to the variations (44) of the Dirac line,

$$S_{gf}^{min}(\theta^{phot},j)=\min_{ds=0}S_{gf}(\theta^{phot},p[j]+s). \tag{45}$$

If the photon field is absent, the minimum (45) is given by the Dirac line with minimal ''Coulomb interaction'' [c.f. Eq. (43)]. For a lattice monopole and antimonopole separated along one axis this line is the shortest path connecting the pair.

We substitute the FP unity (36),(42) into the partition function of compact electrodynamics,

$$Z=\int_{-\pi}^{\pi}\mathcal{D}\theta e^{-S(\theta)}; \tag{46}$$

then we transform the gauge field $\theta\to\theta^{(-\omega)}$ and get the product of the gauge orbit volume $\int\mathcal{D}\omega$ and the partition function within the fixed gauge,

$$Z_{gf}=\int_{-\pi}^{\pi}\mathcal{D}\theta e^{-S(\theta)-\lambda||\theta||^2}\Delta_{FP}[\theta;\lambda]. \tag{47}$$

Separating the gauge field into the monopole and photon parts as indicated by Eq. (40) and using the Hodge–de Rahm transformation, one can show that

$$||\theta||^2=(\delta\theta^{phot},\Delta^{-1}\delta\theta^{phot})+(d\theta^{phot}+2\pi p[j],\Delta^{-1}(d\theta^{phot}+2\pi p[j]))-4\pi^2(j,\Delta^{-2}j). \tag{48}$$

According to Eqs. (42),(45),(47) the only nonvanishing contribution to the partition function in the limit $\lambda\to\infty$ comes from the global minimum (48) in the gauge orbit. Comparison of Eqs. (45) and (48) shows that this minimum is defined by the following conditions:

$$\delta\theta^{phot}=0 \tag{49}$$

together with

$$S_{gf}(\theta^{phot},p[j])=S_{gf}^{min}(\theta^{phot},p[j]), \tag{50}$$

where S_{gf} and S_{gf}^{min} are given in Eqs. (43) and (45), respectively.

In the continuum limit the condition (49) leads to the usual Landau gauge condition

$$\partial_\mu A_\mu^{phot}=0, \tag{51}$$

while the condition (50) can be formulated as a requirement for the Dirac lines to form a configuration with as small a length as possible:

$$\min_{\delta^* p[j]=\delta j} \text{length}(p[j]). \tag{52}$$

Indeed, the Dirac lines $^*p[j] = {}^*p_1[j] + {}^*p_2[j] + \ldots$ correspond to singular δ functions in the continuum limit. Here $^*p_i$ correspond to mutually unconnected pieces of these lines. The self-interaction of the Dirac lines in Eq. (50), $\Sigma_i(^*p_i[j], \Delta^{-1} {}^*p_i[j])$, contains the term $\alpha \Sigma_i \text{length}(p_i[j])$ (with a logarithmically divergent coefficient α) plus finite terms. The ''Coulomb interaction'' of different pieces of the Dirac lines, $(^*p_i[j], \Delta^{-1} {}^*p_k[j])$, $i \neq k$, as well as the contribution of the regular fields to the condition (50) are finite in the continuum limit. Thus the only essential contribution to the condition (50) in the continuum limit is given by the term $\alpha \Sigma_i \text{length}(p_i[j]) \equiv \alpha \text{ length}(p[j])$, which gives the condition (52).

Thus we conclude that in the continuum limit the minimal Landau gauge for the compact gauge fields is reduced to the local gauge condition (51) for the regular fields and a nonlocal condition (52)—the requirement for the total length of the Dirac lines to be as small as possible—for the singular fields. This result can easily be generalized to the 4D case.

IV. NUMERICAL ALGORITHMS USED IN THE ANALYSIS

A. Monte Carlo updating

The Monte Carlo algorithm in use for this investigation is a mixture of local and global updates. The local Monte Carlo algorithm is based on a five-hit Metropolis update sweep in an even-odd fashion, alternating with a microcanonical sweep, also in checkerboard mode. Both together are considered as *one* local update. After three local updates the Metropolis step width is eventually tuned to keep an acceptance in the range between 40% and 60%.

For better ergodicity, in particular in the presence of an external field (considered in Ref. [6]), global updates have also been included, following the ideas of Ref. [13]. In the equilibrium regime, after every three complete local updates, a global refreshment step is attempted. We try to add one unit of flux to the dynamical gauge field, with random sign in one of the three directions randomly selected. The proposed flux addition is subject to a global Metropolis acceptance check.

For example, one unit of flux in the $\mu\nu$ plane is introduced with the help of the following gauge field shift [13] $\theta_{x,\mu} \to [\theta_{x,\mu} + \tilde{\theta}_{x,\mu}]_{\text{mod}2\pi}$:

$$\tilde{\theta}_{x,\nu} = \frac{\pi}{L_\mu}(2x_\mu - L_\mu - 1),$$

$$\tilde{\theta}_{x,\nu} = 0 \quad \text{for} \quad x_\nu \neq L_\nu,$$

$$\tilde{\theta}_{x,\mu} = \frac{2\pi}{L_\mu} L_\nu (1 - x_\nu), \quad \tilde{\theta}_{x,\rho} = 0, \quad \rho \neq \mu, \nu. \tag{53}$$

The acceptance rate of the global step changes with β in a different way depending on the lattice geometry. In our $T = 0$ studies (on 32^3 lattices) we found that the acceptance of global update steps drops (more rapidly than exponentially) from 0.48 at $\beta = 1.0$ to 0.0056 at $\beta = 2.0$. For higher β essentially no global offers are successful.

In our $T \neq 0$ studies on $32^2 \times 8$ lattices, however, we found the acceptance changing smoothly (nearly exponentially, even across the deconfining transition) from 0.58 at $\beta = 1.0$ to 0.18 at $\beta = 3.0$. A closer look reveals that the higher acceptance rate is due to more frequent global changes of the flux penetrating the 12 plane (i.e., magnetic flux direction).

In summary, one total Monte Carlo update cycle consists of three cycles of local update, each consisting of a Metropolis sweep followed by a microcanonical sweep, interchanging with a global update as described above.

In the finite-temperature case, the measurement of D_T turns out to be highly sensitive with respect to insufficient removal (by the gauge-fixing procedure and its repetitions; see the next subsection) of Dirac strings wrapping around the third direction. This is a case where the results with and without global updates, mainly adding and subtracting fluxes through the 12 plane, differ. We comment on this problem and how to deal with it in Sec. VI.

B. Landau gauge fixing

The Landau gauge has been chosen first of all because it is the most popular gauge to define a gauge field propagator. In this gauge the gauge propagator (5) is expected to satisfy the transversality condition

$$F(q^2) = q_\mu D_{\mu\nu}(\vec{q}) q_\nu \equiv 0. \tag{54}$$

In the case of zero temperature, for example, this allows one to describe the propagator by a single function $D(q^2)$ alone, defined by

$$D_{\mu\nu}(\vec{q}) = \left(\delta_{\mu\nu} - \frac{q_\mu q_\nu}{q^2} \right) D(q^2). \tag{55}$$

We will see that for any practical implementation of the Landau gauge Eq. (54) is slightly violated. This degree of violation can, however, be easily controlled by sharpening the convergence criteria of the gauge-fixing algorithm. More important is the remark that in the case of the angle definition of the vector potential (6) it is really necessary to select the transverse part by projection using Eqs. (15) and (16). Then it is interesting to see where (e.g., in momentum space) the violation of transversality, quantified by the longitudinal propagator F, is coming from.

There is a second reason to choose the Landau gauge. We intend to split the gauge field into a regular (photon) and a singular (monopole) part by reconstructing the field due to the Dirac plaquettes which, on the other hand, are forming the monopoles. This reconstruction becomes unique in the Landau gauge.

In order to implement the gauge-fixing condition (33) we have chosen a mixture of overrelaxation and nonperiodic gauge transformations [14], both applied in alternating order.

Iterative overrelaxation has to be practiced in a checkerboard fashion. Starting, say, with the odd sublattice, we have

first to find for each odd site $\vec{n}$ a suitable $\omega_{\vec{n}}$ which maximizes the following function of ω:

$$\mathcal{G}^{loc}_{\vec{n}}(\theta,\omega)=\sum_{\mu}\left[\cos(\theta_{\vec{n},\mu}-\omega_{\vec{n}})+\cos(\theta_{\vec{n}-\vec{\mu},\mu}+\omega_{\vec{n}})\right], \tag{56}$$

which represents the part of $\mathcal{G}$ actually depending on $\omega_{\vec{n}}$, and second to perform immediately the updatings of the neighboring link angles

$$\theta_{\vec{n},\mu}\rightarrow\theta_{\vec{n},\mu}-\omega_{\vec{n}},$$

$$\theta_{\vec{n}-\vec{\mu},\mu}\rightarrow\theta_{\vec{n}-\vec{\mu},\mu}+\omega_{\vec{n}}. \tag{57}$$

This can be done simultaneously for half the sites, namely, $\vec{n}\in\Lambda_{odd}$. Afterward the same procedure is applied to the even sublattice. One odd or even pair of gauge updates constitutes one single iterative overrelaxation step. Each overrelaxation iteration is followed by a zero-mode subtraction (to be explained in the next subsection).

The angle $\omega_{\vec{n}}$ can be easily found as

$$\tan(\omega_{\vec{n}})=\frac{\sum_{\mu}\left[\sin(\theta_{\vec{n},\mu})-\sin(\theta_{\vec{n}-\vec{\mu},\mu})\right]}{\sum_{\mu}\left[\cos(\theta_{\vec{n},\mu})+\cos(\theta_{\vec{n}-\vec{\mu},\mu})\right]}. \tag{58}$$

These gauge angles are multiplied by the overrelaxation factor $\omega_{\vec{n}}\rightarrow\eta\omega_{\vec{n}}$ and bounded by $|\omega_{\vec{n}}|<\pi$ before the iteration (57) is performed on all links. A good overrelaxation parameter has been found to be $\eta=1.8$. According to our experience from studies on 16^3 lattices this η leads to the fastest convergence, almost independently of β. This value was then applied for all iterative gauge fixings.

The overrelaxation will usually be stopped if in the last overrelaxation step the average increase of the gauge functional $\mathcal{F}$ [Eq. (32)] per link is found to be less than 10^{-6}. After this has been discovered, the gauge fixing procedure ends with a final zero-mode subtraction (see below).

At any *local extremum* of $\mathcal{F}$ [Eq. (32)] the following condition would be satisfied everywhere on the even *and* odd sublattices:

$$(\partial_\mu A_\mu)_{\vec{n}}\equiv\sum_{\mu}\left(A_{\vec{n}+(1/2)\vec{\mu},\mu}-A_{\vec{n}-(1/2)\vec{\mu},\mu}\right)$$

$$\equiv\frac{1}{ga}\sum_{\mu}\left[\sin(\theta_{\vec{n},\mu})-\sin(\theta_{\vec{n}-\hat{\mu},\mu})\right]=0. \tag{59}$$

Having the vector potential localized on the midpoints of links, its divergence is naturally defined on sites $\vec{n}$. Exact vanishing of the divergence of A_μ can be expected in the result of Landau gauge fixing only for the sine definition of the vector potential A_μ.

The algorithm outlined above will not in general lead to the absolute (global) maximum of the gauge functional $\mathcal{F}$ [Eq. (32)]. Typically it will get stuck in one of the local maxima, which are called Gribov copies of the true maximum. This is the so-called Gribov problem. It is partially cured by repeating the same gauge-fixing procedure, applying it to random gauge copies of the original Monte Carlo configuration θ^{MC}, assuming that one of these copies might be situated in the basin of attraction of the true maximum. The number of gauge equivalent configurations produced to restart the gauge fixing is denoted as N_G and iterative gauge fixing generically leads to really different maxima. We have then to be content with the *best out of all* N_G+1 *local maxima* of the gauge functional. The convergence, with increasing N_G, of a gauge dependent quantity evaluated on a given gauge field ensemble with the help of the best Gribov copy gives an indication of the sensitivity of this quantity with respect to the misidentification of the true maximum. We have applied this philosophy to two sets of data, the propagator data themselves at large or small momenta, and the fit parameter emerging from a fit of the gauge boson propagator. One should not be surprised that the number N_G that is necessary to achieve uniform convergence of the propagator in momentum space and/or of the fit parameters differs strongly between zero and finite temperature. At finite temperature there are strong differences between D_L and D_T.

In Sec. III we stressed the importance of finding a local maximum of Eq. (32) accompanied by a minimal length of Dirac strings. Within our implementation, the start from a new random gauge copy is done in the hope of producing a new Gribov copy reachable from the previous ones only by a discrete gauge transformation. We have monitored the number of Dirac strings in each of the local maxima of the gauge functional $\mathcal{F}$ [Eq. (32)]. Each time the recent best value of the gauge functional was replaced by a better (higher) one, the number N_D of Dirac strings detected in the correspondingly best Gribov copy decreased compared to the previous one.

In Fig. 1 we show scatter plots relating the gauge functional $\mathcal{F}$ to the number of Dirac strings per direction N_i^D ($i=1,\ldots,3$) for two reduced ensembles of 100 out of 1000 equilibrium configurations on $32^2\times 8$ lattices, each of them starting with 101 Gribov copies (local maxima of $\mathcal{F}$). Figure 1(a) refers to $\beta=2.0$ (confined phase) and shows all local maxima (Gribov copies). The isotropy of the Dirac strings is clearly visible. Figure 1(b) shows how in the deconfined phase the number N_3^D of temporal Dirac strings is correlated with the locally maximal value of $\mathcal{F}$. Figure 1(c) shows it for N_1^D and N_2^D (number of spatial Dirac strings). In both cases a slight tendency to clustering near multiples of 8 or 32 (the respective periodicities of the lattice) is visible, in particular for the highest values of $\mathcal{F}$. The selection of the best copies restricts the ensemble to bigger $\mathcal{F}$ and smaller N_i^D as shown in Fig. 1(d). In the confinement phase the Dirac strings are still approximately isotropic. In the deconfined phase, however, the highest values of $\mathcal{F}$ are correlated with low multiplicity of N_1^D and N_2^D, and N_3^D corresponding to zero, with one or a few periodically winding Dirac strings more frequently in the temporal direction.

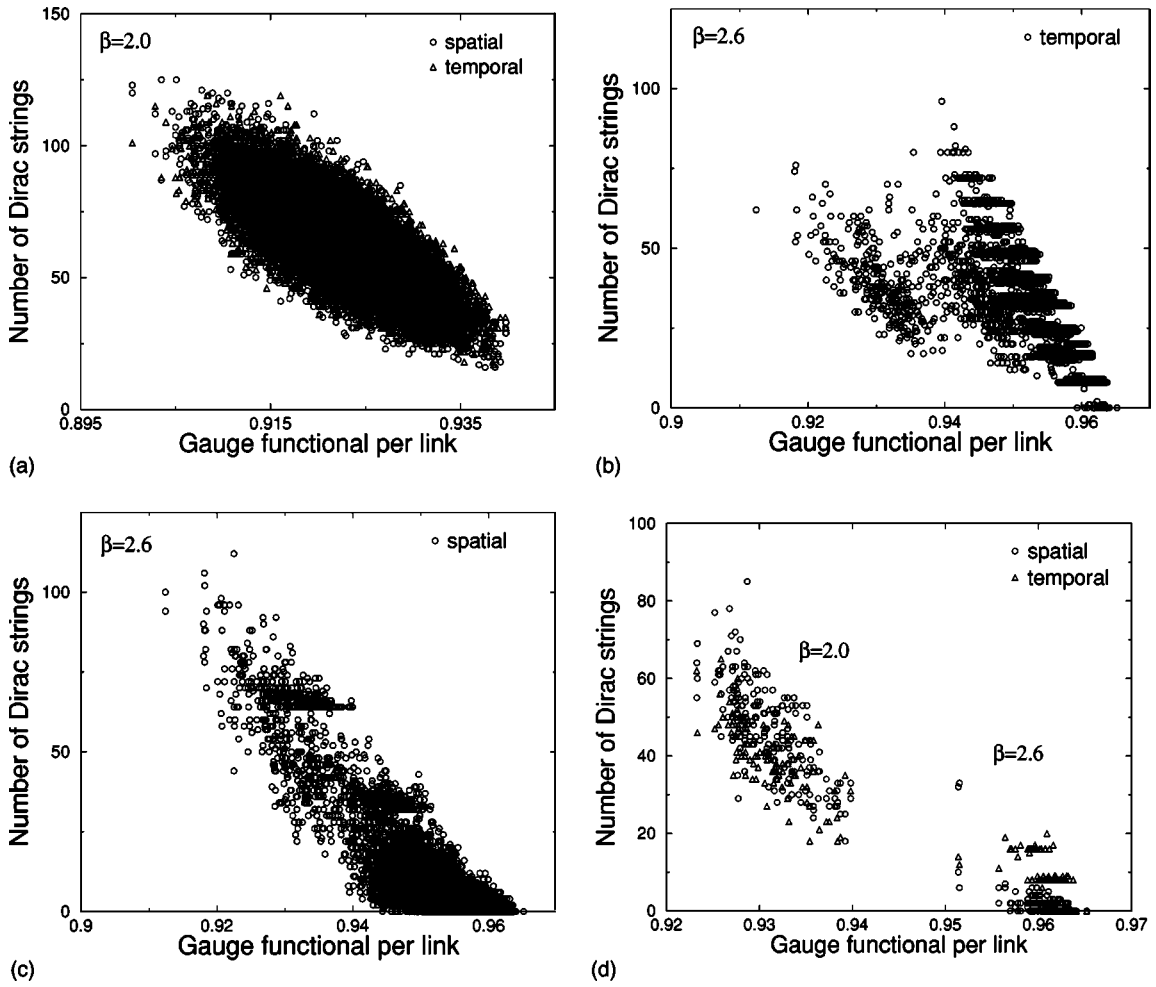

FIG. 1. Scatter plots of the average gauge functional $\mathcal{F}(\theta)$ per link and the related number of Dirac strings in the *temporal* (N_3^D) and/or the *two spatial* (N_1^D and N_2^D) directions for 100 configurations on a lattice $32^2\times 8$: (a) N_3^D, N_1^D, and N_2^D vs $\mathcal{F}(\theta)$ in the confinement phase ($\beta=2.0$), each configuration represented by 101 Gribov copies; (b) N_3^D vs $\mathcal{F}(\theta)$ in the deconfinement phase ($\beta=2.6$); (c) same as in (b) for N_1^D and N_2^D; (d) the two samples represented only by the best out of 101 Gribov copies.

We stress that the configurations of which the gauge fixing has been investigated here in some detail were produced with the update algorithm including global updates. Winding Dirac strings of some lifetime are also produced in ensembles that are generated *without* global updates, but less frequently. Therefore, the inefficiency of the random gauge transformation in exploring more of the gauge orbit is a handicap also if global updates are suppressed. We will see later that certain problems which show up in the finite-temperature propagator D_T can be ameliorated, but not completely cured, by abandoning global updates and increasing the number of Gribov copies.

We had not the opportunity to reconstruct exactly the spatial conformation of the Dirac strings in each gauge copy. But for each gauge copy we can determine whether multiple Dirac strings (running along a certain direction with the same or different orientation) can be definitely excluded or not. At low β this can never be excluded, but at high β this could be used as an additional criterion to reject Gribov copies that contain double Dirac strings (in the case of two *oppositely* oriented strings).

Although the stopping criterion was formulated for a global increase of $\mathcal{F}$ we did not find a systematic local variation, depending on the distance from a monopole, of the violation of Eq. (59), expressed by the quantity

$$(\partial_\mu A_\mu)_n^2 \equiv \left\{ \sum_\mu \left(A_{\vec{n}+(1/2)\vec{\mu},\mu} - A_{\vec{n}-(1/2)\vec{\mu},\mu}\right)\right\}^2 . \qquad (60)$$

This suggests that the differential gauge condition (59) uniformly approaches zero.

In contrast to this, we found a systematic local variation of the local gauge functional itself,

$$\mathcal{F}_{\vec{n}}^{loc}(\theta) = \sum_\mu \left[\cos(\theta_{\vec{n},\mu}) + \cos(\theta_{\vec{n}-\vec{\mu},\mu})\right], \qquad (61)$$

with the distance from a monopole. Near to a monopole, its value is suppressed compared to the bulk average. This is illustrated in Fig. 2 for $\beta=1.0$ and $\beta=2.0$.

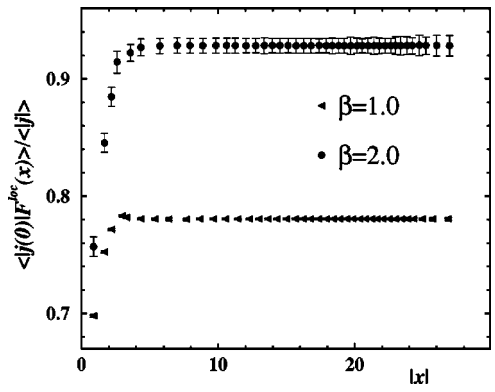

FIG. 2. Suppression of the local gauge functional $\mathcal{F}^{loc}_{\vec{n}}$ near a monopole for $\beta=1.0$ and $\beta=2.0$. For better presentation some of the data points are not plotted. Notice the β dependence of the bulk average of $\mathcal{F}^{loc}_{\vec{n}}$.

C. Zero-mode subtraction

There are certain modes of the gauge field which are not suppressed by the action. If they are not taken care of properly, the gauge field propagator is known to be spoiled [14]. For instance, adding some constant to all link angles $\theta_{\vec{n},\mu}$ in one particular direction does not change the action (1), and neither does adding a multiple of 2π to one particular link angle. Nonperiodic gauge transformations can be considered to implement these changes. We have used them in our simulations to immediately eliminate zero modes related to the appearance of the volume average of the link angles in a given direction,

$$\overline{\theta_\mu}=\sum_{\vec{n}}\ \theta_{\vec{n},\mu}/|\Lambda|, \tag{62}$$

where $|\Lambda|$ is the lattice volume. We subtract this volume average from each link angle $\theta_{\vec{n},\mu}$ in the μ direction,

$$\theta_{\vec{n},\mu}\to\theta_{\vec{n},\mu}-\overline{\theta_\mu}+2\pi k, \tag{63}$$

with integer k chosen such that $\theta^g_{\vec{n},\mu}\in(-\pi,\pi]$. This operation can be imagined as resulting from a gauge function $g_{\vec{n}}=-\overline{\theta_\mu}n_\mu$ (no summation) which is in general nonperiodic. This special sort of gauge fixing is completed when zero modes in all d directions have been subtracted.

The zero-mode subtraction step is applied after each overrelaxation step. Thus it is always performed before the measurements are done on the gauge-fixed configuration.

In our runs we measured the photon propagator after each tenth total Monte Carlo update cycle to avoid autocorrelations as much as possible. Typically, we used 500 gauge-fixed configurations per data point for the 32^3 lattice and about 2000 configurations for the $32^2\times 8$ lattice.

V. THE ZERO-TEMPERATURE PROPAGATOR IN THE LANDAU GAUGE

In coordinate space, the gauge boson propagator that is studied reads

$$D_{\mu\nu}\left(\vec{m}+\frac{1}{2}\vec{\mu}-\vec{n}-\frac{1}{2}\vec{\nu}\right)=\langle A_{\vec{m}+(1/2)\vec{\mu},\mu}A_{\vec{n}+(1/2)\vec{\nu},\nu}\rangle \tag{64}$$

with the angle or sine definition of A. For brevity, we will refer to this propagator later in momentum space as $D^{ang}_{\mu\nu}$ or $D^{sin}_{\mu\nu}$. The two scalar functions occurring in momentum space [Eq. (10)] we will denote as D^{ang} and F^{ang} or D^{sin} and F^{sin}, respectively. The last one, F^{sin}, should vanish in the Landau gauge. We have observed that this is indeed the case with an accuracy determined by the stopping criterion of the iterative overrelaxation. For the sine propagator the transverse part can be calculated directly just by evaluating and summing the diagonal components appearing in Eq. (16). When the longitudinal propagator vanishes only approximately, one can extract the transverse propagator following Eqs. (15),(16).

In Fig. 3 we show the different forms of the transverse propagator D^{sin} and its components as well as the vanishing

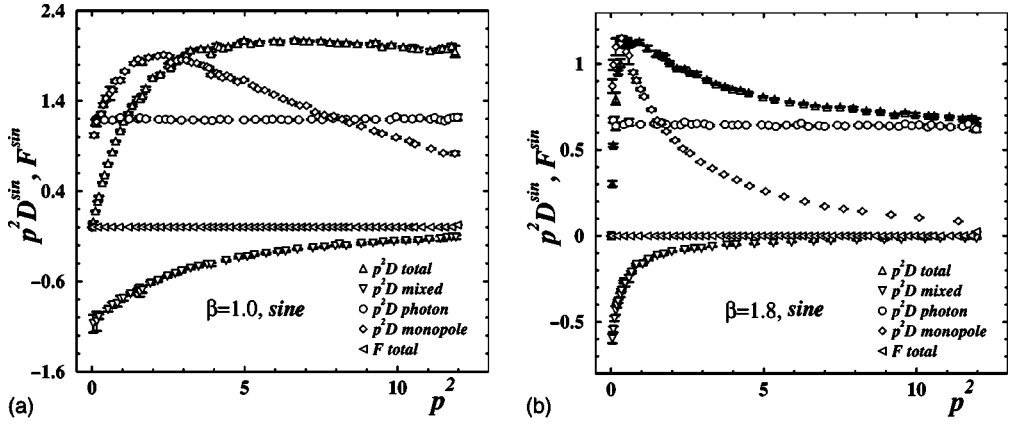

FIG. 3. The Landau gauge sine propagator as a function of p^2 measured on a 32^3 lattice. For the transverse part p^2D^{sin} [(a) at $\beta=1.0$ and (b) at $\beta=1.8$] we show the full propagator, the singular (mono), the regular (phot), and the mixed contribution for comparison. In addition, we show the (vanishing) longitudinal propagator F^{sin}. The data represent the evaluation of $N_G=20$ gauge copies. For better presentation some of the data points are not plotted.

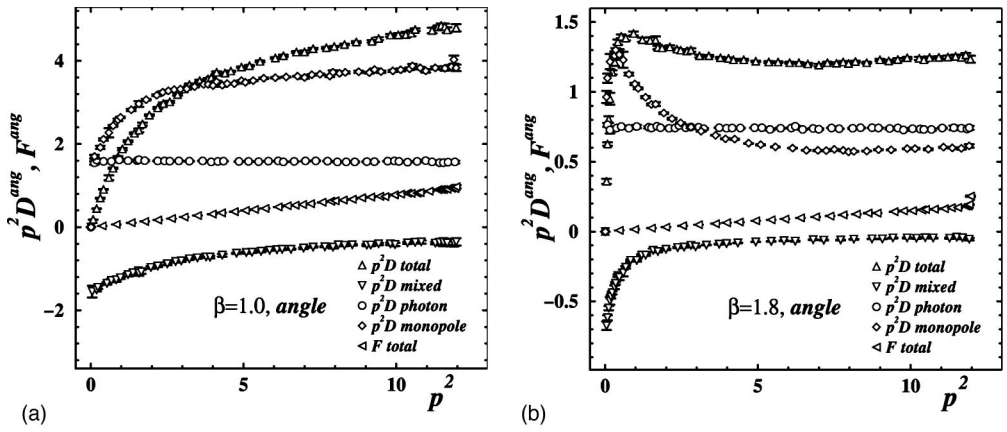

FIG. 4. The same as in Fig. 3 for the Landau gauge angle propagator. Notice the nonvanishing longitudinal propagator F^{ang} decreasing with growing β.

longitudinal propagator F^{sin}. These data were obtained on a 32^3 lattice for (a) $\beta=1.0$ and (b) $\beta=1.8$, with $N_G=20$ Gribov copies evaluated in addition to each original Monte Carlo configuration. The data at other β were produced under the same conditions. In Fig. 4 the same is presented for D^{ang}, its components, and nonvanishing F^{ang}.

For the angle definition of A_μ, the decomposition into components is strictly additive [Eq. (31)]. We have observed that the longitudinal propagator F^{ang} and its components are well described by the form $F(p^2)=Pp^2$, where P is a constant. We find that $F^{ang,phot}$ essentially coincides with the full F^{ang}. The size of F^{ang} and its photon component is of the same order of magnitude as the transverse part at $\beta=1.0$, while the monopole and mixed parts are one order of magnitude smaller. At $\beta=1.8$, the size of F^{ang} and its photon component is an order of magnitude smaller than at $\beta=1.0$, while the monopole and mixed parts are negligible.

For the sine definition of A_μ, the monopole part of the transverse propagator $D^{sin,mono}$ has a maximum in the low momentum region (which moves more and more toward $p^2=0$ with higher β) before it drops toward $p^2=0$. For the angle definition, a maximum of $D^{ang,mono}$ develops only for $\beta>1.0$.

Summarizing, we have observed that the longitudinal part F is either zero (for the sin θ definition of the gauge field in the correlator) or it is nonzero, and then it coincides with its photon part (for the θ definition). Therefore, at zero temperature the Landau gauge propagator $D^{ang}_{\mu\nu}$ is not completely transverse. This is entirely due to the difference between the definitions of the vector potential. This discrepancy, expressed by the nonvanishing F^{ang}, becomes ameliorated at higher β.

For both definitions of A_μ we find that the regular (photon) part of the transverse propagator is singular at $p^2\to 0$, like $D^{phot}\sim 1/p^2$, while the full transverse propagator is not. Following Ref. [7] we try to describe the two by functions of the form

$$D(p^2)=\frac{Z}{\beta}\,\frac{m^{2\alpha}}{p^{2(1+\alpha)}+m^{2(1+\alpha)}}+C \tag{65}$$

and

$$D^{phot}(p^2)=\frac{Z^{phot}}{\beta}\,\frac{1}{p^2}+C^{phot}. \tag{66}$$

The model function (65) is similar to some of the functions discussed in Refs. [15,16] where the propagator in gluodynamics was studied. In the case of $T=0$ we expect these two curves to differ *at all* β in order to accommodate the (permanent) confinement property of the model. Figure 5(a) shows the anomalous dimensions α first increasing in the low-β region. The anomalous dimensions for the angle and for the sine propagator behave quite similarly to each other (the dimension for the angle propagator is a bit smaller). As β gets larger than $\beta\sim 1.5$ the anomalous dimensions start to descend toward zero. This indicates that the anomalous dimension is not only a function of the monopole density, which decreases monotonically with growing β for all values of the coupling. The (cluster) structure of the monopole configurations may play a significant role for α.

In Fig. 5(b) the mass parameters m are presented for the angle and sine propagators according to Eq. (65) as a function of β. Both masses are almost equivalent. For the mass there exists a theoretical prediction due to Polyakov [1],

$$m_{th}(\beta)=2\pi\sqrt{2\beta}\exp\{\pi^2\beta_V(\beta)\Delta^{-1}(0)\}, \tag{67}$$

where β_V is the Villain coupling constant

$$\beta_V(\beta)=\left[2\log\left(\frac{I_0(\beta)}{I_1(\beta)}\right)\right]^{-1}. \tag{68}$$

$I_0(\beta)$ and $I_1(\beta)$ are modified Bessel functions and β is the Wilson action coupling constant appearing in Eq. (1). The prediction (67) is valid for a dilute monopole gas. The agreement between the two data sets and the theoretical curve is very good. The small deviation at lowest β can be attributed to violation of the dilute gas approximation.

Figure 5(c) shows $Z(\beta)$ and $Z^{phot}(\beta)$ for the two definitions. We observe that Z tends to unity at large β, whereas

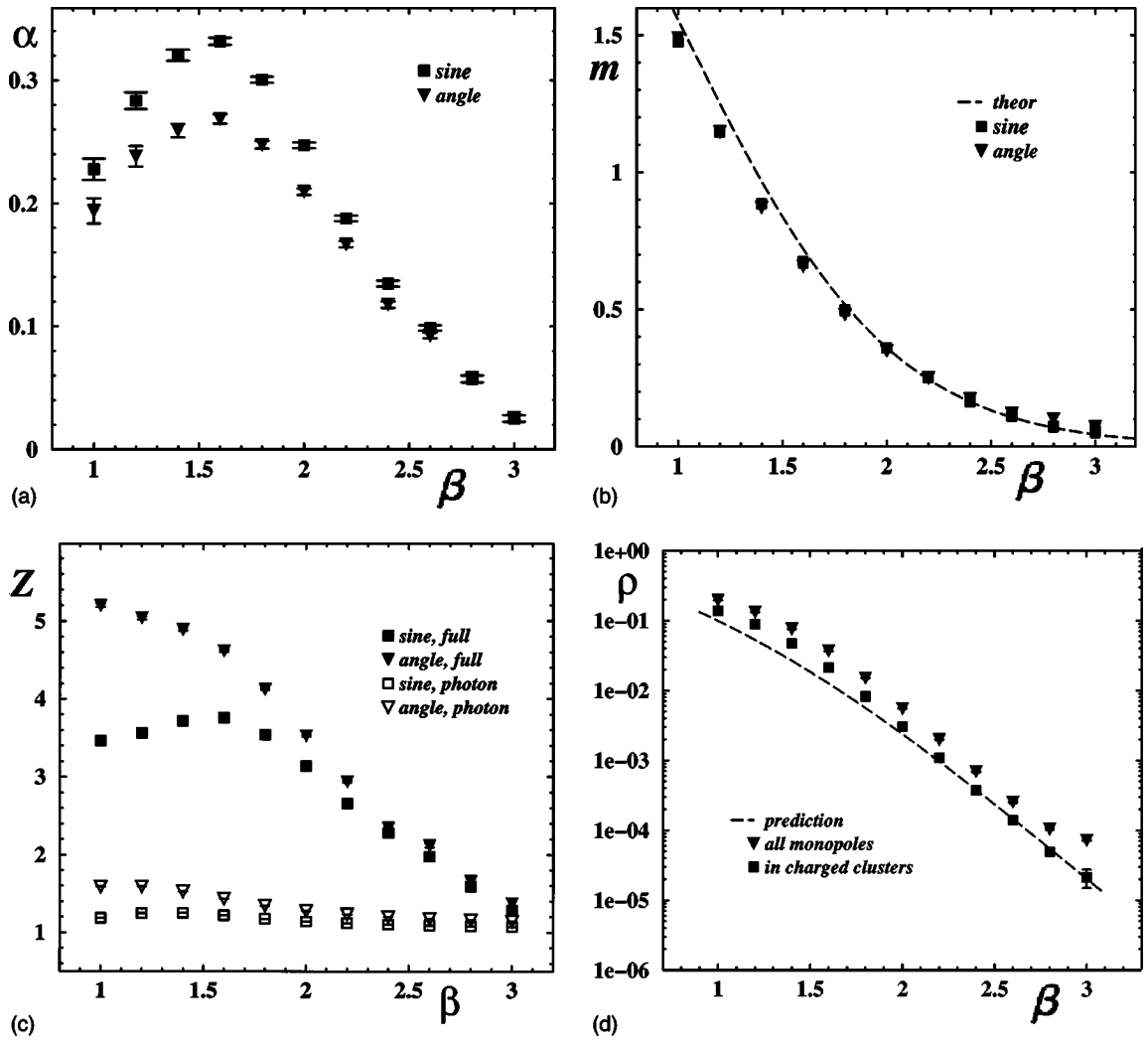

FIG. 5. The best fit parameters for the zero-temperature sine and angle propagators as functions of β: (a) the anomalous dimension α; (b) the mass parameter m with the theoretical prediction [Eq. (67)] as dashed line; (c) the parameters Z and Z_{phot} [using Eq. (65),(66)]; (d) the total monopole density and the monopole density in charged clusters with the theoretical prediction [Eq. (69)].

$Z^{phot}(\beta)\approx 1$ for all β. The strong deviation of Z from unity at small β can be interpreted as a field renormalization by the monopoles.

The simplest quantity characterizing the monopoles is the monopole density $\rho=\Sigma_c j_c/|\Lambda|$, where the monopole charge j is defined in Eq. (41). Note, however, that a general monopole ensemble may contain lattice artifacts which at zero temperature are realized in the form of ultraviolet monopole-antimonopole pairs. Following Ref. [5] we remove these lattice artifacts using a cluster analysis. For our purposes, clusters are defined as connected groups of monopoles and antimonopoles, where each object is separated from at least one neighbor belonging to the same cluster by a distance less than or equal to $R_{\max}$. We use $R^2_{\max}=3a^2$ which means that neighboring monopole cubes should share at least one single corner. The cluster is called charged if the total charge of its constituent monopoles is nonzero. This includes isolated monopoles and antimonopoles.

In Fig. 5(d) we plot the measured total monopole density and the density of monopoles residing in charged (physical) clusters. The charged fraction is well described by the theoretical formula for the monopole density,

$$\rho(\beta)=2\exp\{-2\pi^2\beta_V(\beta)\Delta^{-1}(0)\}, \tag{69}$$

which is a lattice version [5] of the Polyakov formula [1]. According to Fig. 5 the monopole density, Debye mass, and deviation of the coupling Z from unity are all descending functions vanishing in the limit $\beta\to\infty$.

The contact terms contained in D^{sin} and D^{ang} are not shown here. The photon part of both D^{sin} and D^{ang} vanishes perfectly. The full propagator in both cases contains contact terms C^{sin} and C^{ang}, which deviate from zero for smaller β, whereas always $C^{sin}(\beta)\ll C^{ang}(\beta)$.

The discussion of Figs. 3 and 4 and of the β dependence of the fit parameters in Fig. 5 was based on the zero-temperature propagators (and their components) obtained throughout with $N_G=20$ Gribov gauge copies. The depen-

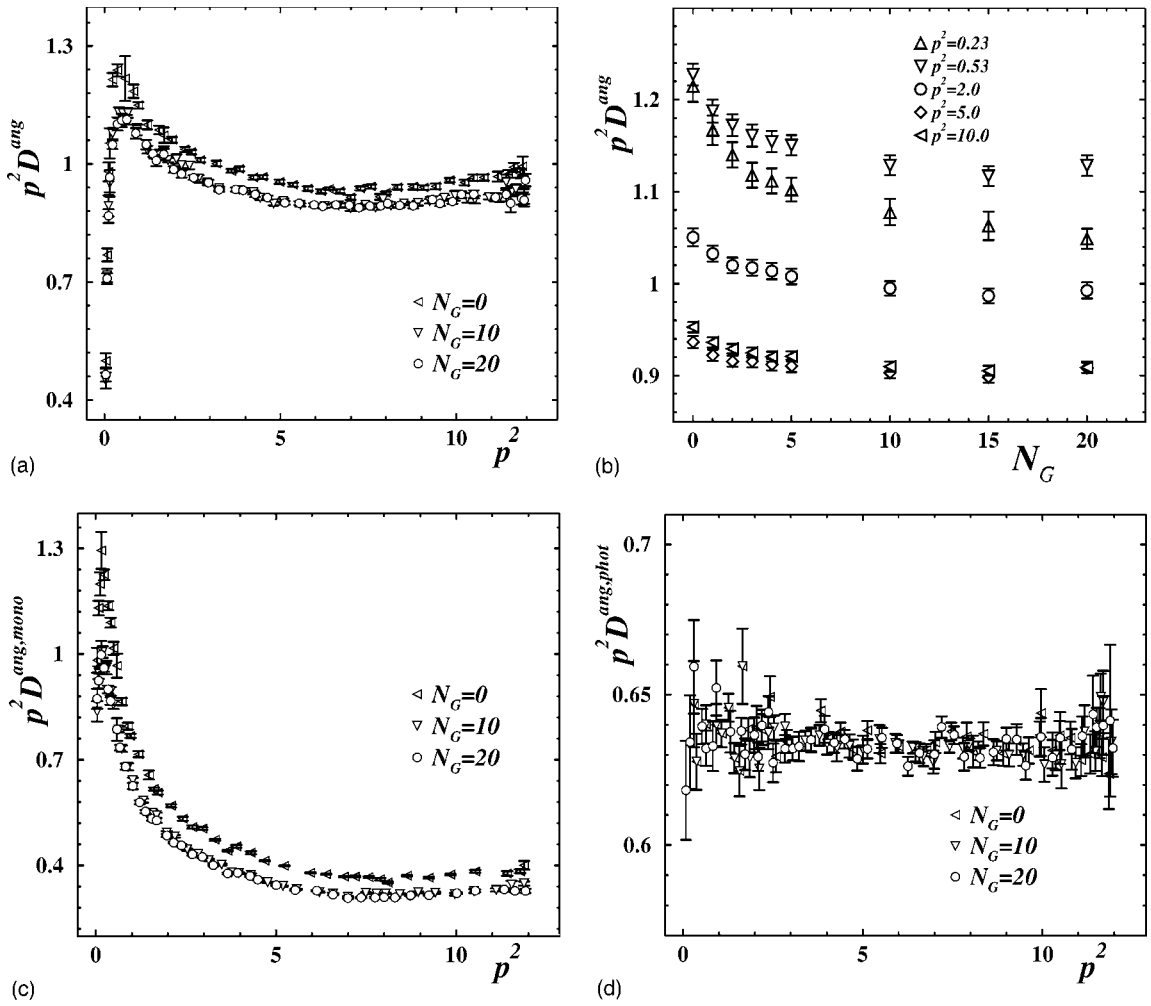

FIG. 6. The dependence of the zero-temperature angle propagator on N_G for a 32^3 lattice (at $\beta=2.0$ as an example) (a) The full transverse propagator for $N_G=0,10,20$ in the full momentum region; (b) its behavior as a function of N_G at five selected momenta; (c) the same for the singular (mono) part of the transverse propagator; (d) the same for the regular (phot) contribution to the transversal propagator. Again for better presentation some of the data points are not plotted.

dence on the number of gauge copies has been investigated carefully for the case of the angle propagator. As a result of this study, the default choice of $N_G=20$ for the gauge-fixing procedure at $T=0$ was established. In Fig. 6 we show different aspects of the approach to the $N_G\to\infty$ limit, for $\beta=2.0$ as an example. Figure 6(a) demonstrates that the transverse propagator evaluated with either 10 or 20 gauge copies is essentially the same, but the naive evaluation (with $N_G=0$) would clearly overestimate the propagator over the whole momentum range. Figure 6(b) shows this in more detail for five selected momenta. It becomes clear that the dependence is strongest in the region of small momenta, in particular the region *below* the peak. The dependence is strong for the singular part presented in Fig. 6(c). Again, there is almost no change between $N_G=10$ and 20. As can be seen from Fig. 6(d), there is almost no N_G dependence in the photon part of the transverse propagator.

We present the resulting dependence of the fit parameters on N_G in Fig. 7, again for $\beta=2.0$. The anomalous dimension α shown in Fig. 7(a) drops by within 10%, which indicates that the anomalous dimension is sensitive with respect to the minimization of the Dirac strings that is achieved by better and better Gribov copies. The mass presented in Fig. 7(b) does not change with N_G, which confirms that it is mainly determined by the monopole mass (i.e., density).[3] Figure 7(c) shows Z for the full transverse propagator and Z^{phot} for the photon part. It is not surprising that the parameter associated with the photon part does not change. The parameter describing the full transverse propagator decreases, again by $\approx 10\%$ within $N_G<20$. One can also observe a slight dependence of Z on N_G for $N_G>20$. However, the dependence is indeed very small (about 1%) and not essential for our qualitative discussion.

From the comparison of the sine propagator and the angle propagator at zero temperature we conclude that the fits of the transverse parts give more or less the same parameters, with a β dependence (if appropriate) which is in accordance with the monopole density. Strict transversality itself is guar-

[3]Let us recall that the monopole positions in a given configuration are gauge independent.

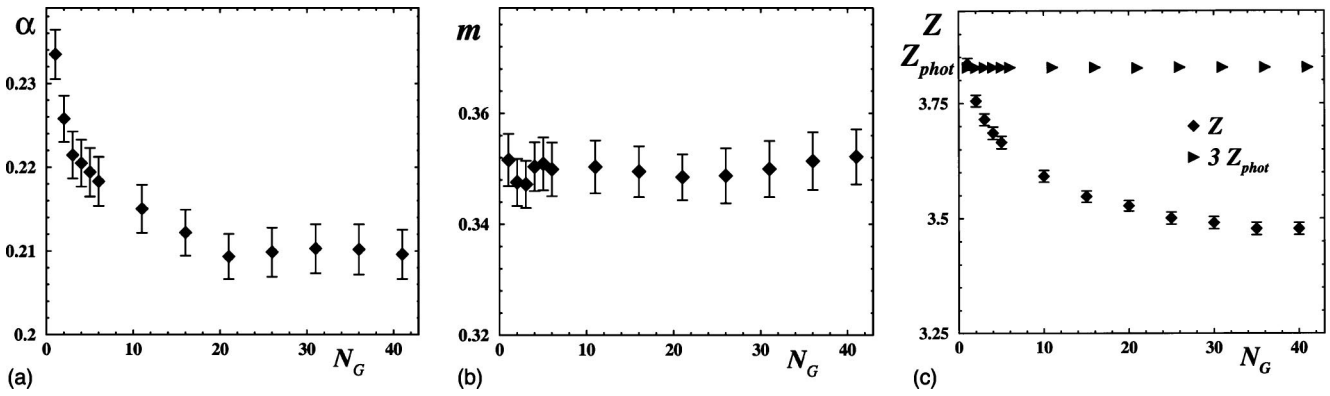

FIG. 7. The best fit parameters for D^{ang} at zero temperature as a function of N_G (for $\beta=2.0$ as an example): (a) Anomalous dimension α, (b) mass parameter m, and (c) renormalization constants Z for D^{ang} and $D^{ang,phot}$.

anteed only in the case of the sine propagator. In the case of the angle definition an appropriate transverse part has to be extracted by the projection (15),(16).

VI. THE FINITE-TEMPERATURE PROPAGATOR IN THE LANDAU GAUGE

In this section we report our investigation of the properties of the gauge boson propagator at finite temperatures. With respect to the distinguished direction $\mu=3$, the propagator D can be separated into transverse and longitudinal components (see Sec. II for the definitions) denoted as D_T and D_L, respectively. We are working on the lattice $32^2 \times 8$, in line with Ref. [7], where only the D_L component of the angle type propagator (with $p_3=0$, $N_G=20$, and a limited statistics of 500 measurements) was studied.

The transverse component of the propagator, D_T, describes the spatial degrees of freedom, while the longitudinal component, D_L, contains gauge fields in the Landau gauge in both the temporal and spatial directions. The finite-temperature propagator data are analyzed again for $p_3=0$, as a function of $\mathbf{p}^2$. In that case D_L is constructed only from temporal degrees of freedom which, in particular, are responsible for the confinement phenomenon. We have fitted the data for both components of the propagator using the fit function (65) invented first in Ref. [7] to describe D_{33}.

First we repeated the investigation of the Gribov copy dependence of the propagator components D_L and D_T, this time for the sine definition of the propagator, similar to that conducted for the zero-temperature case with the angle definition. The results are summarized in Fig. 8 at β values near (below and above) the phase transition. After a few Gribov copy attempts the longitudinal component is almost insensitive to the number N_G. This can be seen from the left panel of Fig. 8. The fitting parameters α_L, m_L, Z_L, and C_L (the last is not shown here) are rapidly converging and become almost independent of N_G for $N_G \gtrsim 7$. The results at large numbers of Gribov copies are not sensitive to whether or not we have suppressed global updates (we made only local updates; see the label ''local '').

The transverse component, however, is strongly dependent on the number of Gribov copies as can be seen from Fig. 8. All the fit parameters α_T, m_T, and Z_T are descending functions of the number of Gribov copies N_G with global updates included. At $N_G=100$ the plateau is not yet reached. Moreover, the results are sensitive to whether or not global updates are included, in particular at high values of β. The measurements with only local updates lead to significantly lower fit results. In deconfinement we would expect vanishing m_T (and α_T), and $Z_T \to 1$.

The reason for that behavior might be explained as follows. On one side, the ''best'' gauge functional is realized in *gauge-fixed* configurations without Dirac lines wrapping around the lattice (predominantly in the short temporal direction). Such Dirac lines are continuously created and destroyed by the Monte Carlo process, even if global updates are not attempted. The level of ''noise'' due to wrapping Dirac lines is higher if global updates are included in the Monte Carlo process, which in general would improve the ergodicity of the system, but it represents a problem also if only local updates are used. The presence of wrapping Dirac strings mimics a finite β-independent lattice mass m_T at larger β, the value of which decreases only with increasing temporal extent L_T. So in the limit of vanishing lattice spacing the dimensionful mass will diverge.

This ''Dirac noise'' represents a serious challenge for the gauge-fixing algorithm. The deterministic part (overrelaxing steepest descent method) described in Sec. IV B cannot remove it. *Unbiased* random gauge transformations applied to get new start configurations for the deterministic search for further Gribov copies are obviously not effective enough to reduce the Dirac noise. A simulated annealing Monte Carlo series of random gauge transformations with the total length of Dirac strings as the ''gauge action'' [17] seems to be more appropriate for selecting new start configurations for the final steepest descent search.

Having these difficulties in mind, we decided to use in the final measurements at finite temperature, for $\beta=2.0$ and larger, only local updates before gauge fixing, and to perform $N_G=100$ Gribov copy attempts. For both sine and angle propagator measurements deep in the confinement phase (below $\beta=2.0$) we used $N_G=20$ and global updates where the results of the zero-temperature analysis for the Gribov copy dependence is applicable, and the fit parameters of both D_L and D_T have to agree within accuracy and should be similar

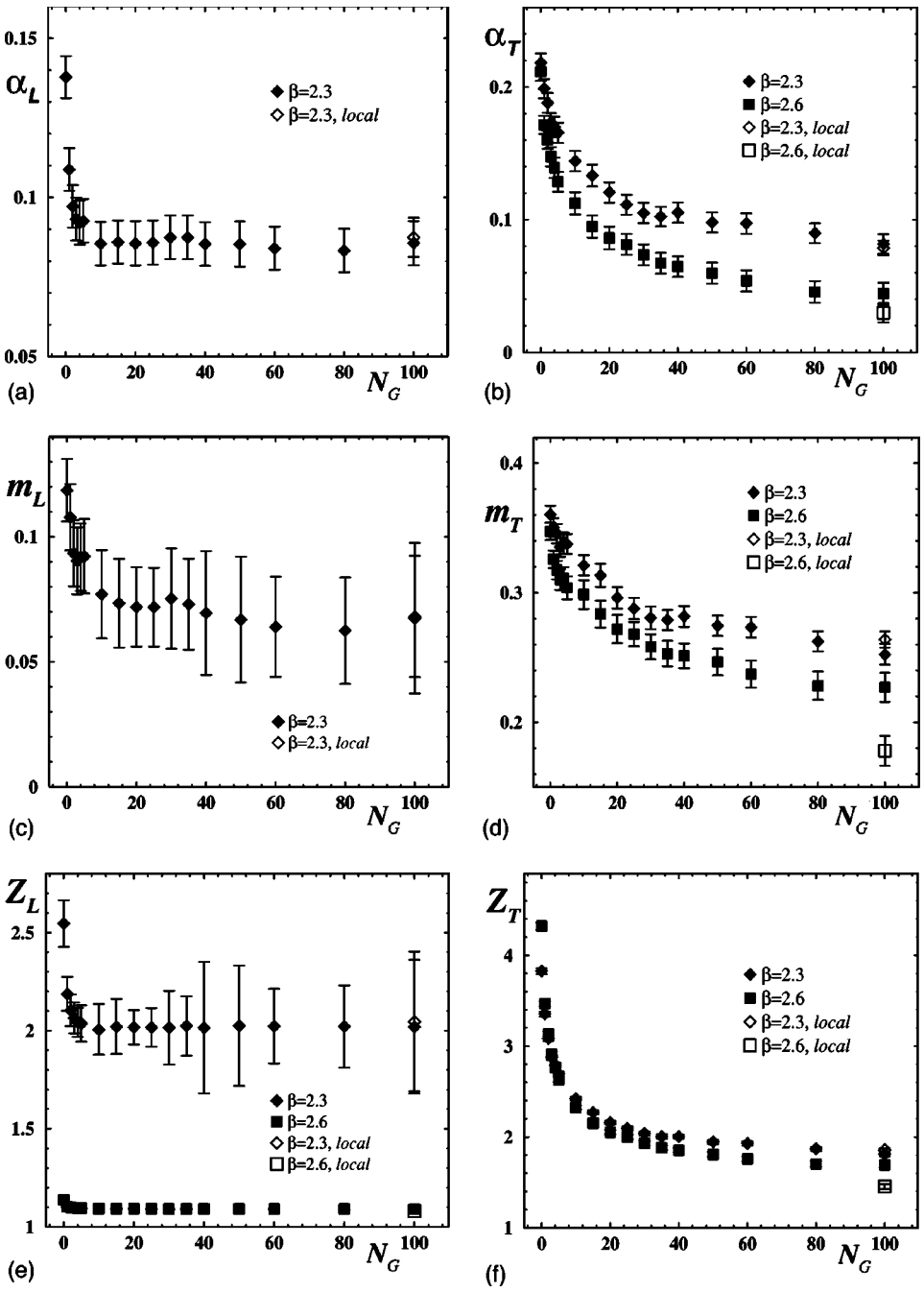

FIG. 8. The Gribov copy dependence of the best fit parameters for the D_L and D_T propagators: the anomalous dimension α (a),(b), the mass parameter m (c),(d) and the parameters Z (e),(f). The label ''local'' corresponds to measurements in Monte Carlo cycles without global updates and with $N_G=100$ extra Gribov copies.

to those for the $T=0$ transverse propagator D. Nevertheless, we have to admit that the results for the transverse propagator D_T should be understood only qualitatively.

The results for the best fit parameters for D_L and D_T are presented in Fig. 9. Let us begin with D_L. At the critical point both the anomalous dimension α_L and the mass m_L vanish while the renormalization parameter Z_L meets the corresponding parameter for the perturbative photon, Z_L^{phot}. This behavior is characteristic for both angle and sine types of propagator and extends our results in Ref. [7]. Note that here also the mass parameters for sine and angle propagators coincide with each other. However, the anomalous dimensions for these cases differ slightly from each other while the renormalization parameters are significantly different, and the renormalization factor for the angle propagator is bigger than that for the sine propagator. The latter is expected because $|\sin\theta|\leqslant|\theta|$.

The corresponding quantities for D_T behave differently for the angle and sine definitions of A_μ, with the remarkable exception of the mass parameter. For example, the anomalous dimension α_T for the angle propagator vanishes in the vicinity of the critical point and beyond, while the same quantity for the sine propagator does not vanish. We explain this behavior as due to insufficient gauge fixing, as can also be guessed from our previous analysis. The same reason explains the fact that the masses m_T for both definitions of the photon propagators—being remarkably similar—do not vanish at the critical point. Finally, for both definitions of the

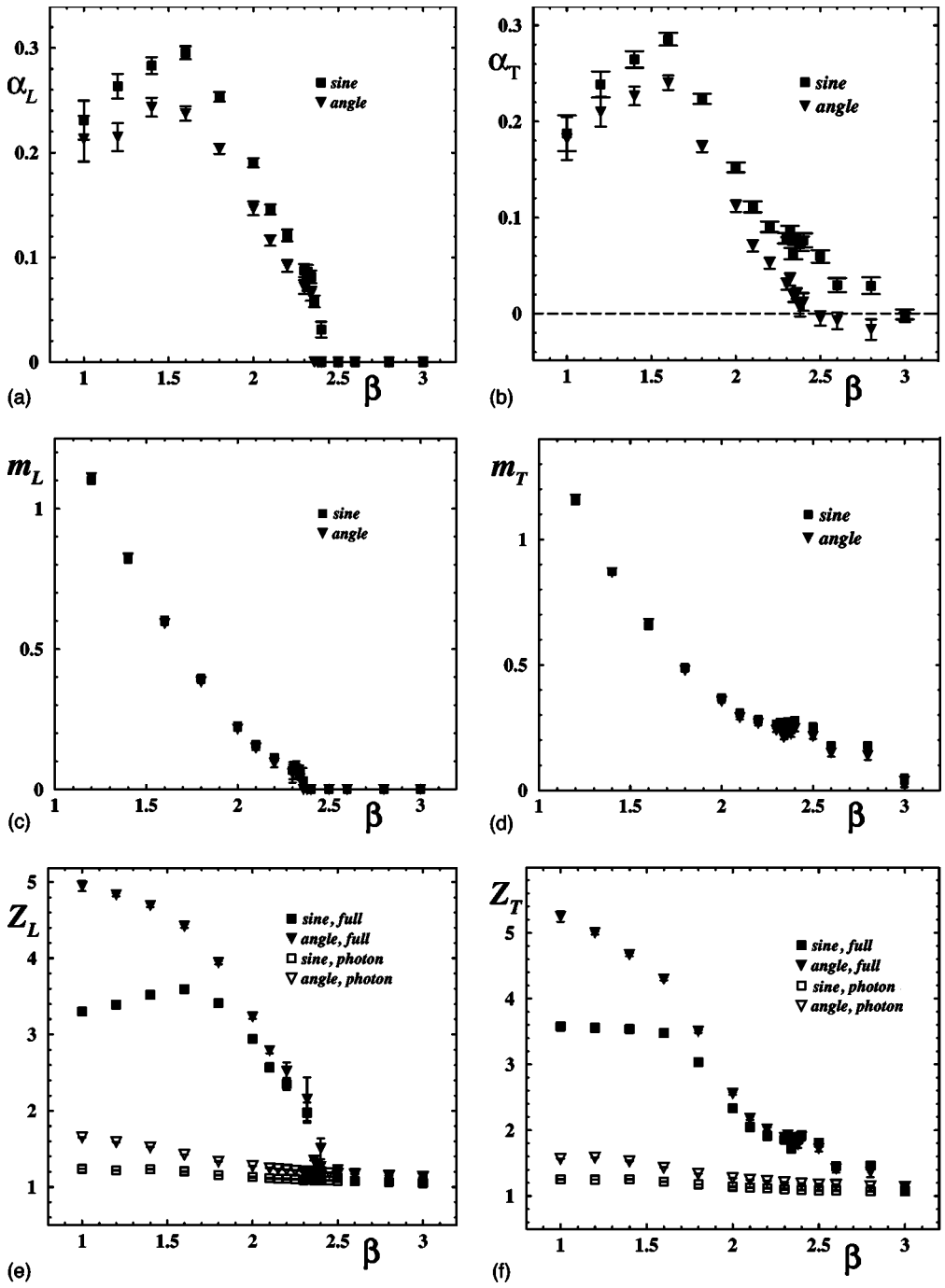

FIG. 9. The best fit parameters for the nonzero-temperature sine and angle propagators as functions of β: the anomalous dimension α (a),(b), the mass parameter m (c),(d), and the parameters Z and Z_{phot} (e),(f). The left column corresponds to D_L, the right to D_T. The fits of full propagators are done with the help of Eq. (65); the photon contribution is fitted by Eq. (66).

propagators the renormalization constants Z_T do not approach the corresponding Z_T^{phot} at the critical point. In order to get reliable behavior of the D_T part of the propagator one should drastically increase the number of Gribov copies used in the gauge fixing. For the time being this is beyond our computing capabilities. The situation could be improved using a variant of the mentioned simulated annealing Monte Carlo series of random gauge transformations in order to choose more appropriate initial gauge transformed configurations before fixing the gauge.

VII. CONCLUSIONS

We studied the gauge boson propagator in cQED$_3$ at both zero and nonzero temperatures. We found that the propagators in all cases under investigation can be fitted by Eq. (65) which is the sum of the massive propagator with an anomalous dimension plus a contact term. Similarly to the case of D_L at finite temperature [7], a nonvanishing anomalous dimension α is also found at $T=0$. Moreover, the fact of the existence of the anomalous dimension is not associated with

a particular type of gauge boson propagator. We have studied angle and sine types of propagator and the corresponding anomalous dimensions are nonvanishing and have a similar behavior to the functions of β.

The existence of the anomalous dimension depends on the presence of the monopole plasma, but it is not directly proportional to the monopole density below $\beta=1.5$. In the confinement phase the monopole plasma is present at any coupling of the system and the density of monopoles is a monotonically decreasing function of the lattice coupling β. A similar behavior is observed for the anomalous dimension in the case of the D_L and D_T propagators. The dimension α_L extracted from the D_L component of the propagator vanishes in the vicinity of the phase transition for both definitions (angle and sine) of the propagator. However, this does not happen for the sine definition of the D_T propagator. We associate this result with an insufficient number of Gribov copies used in the gauge fixing. The D_T propagator requires many more Gribov copies for the gauge fixing than does the D_L propagator.

Concerning the other parameters of the fits, the mass extracted from the propagator at zero temperature and from the D_L propagator at nonzero temperature does not depend on the definition of the propagator. The mass for the $T=0$ case is perfectly described by the Polyakov formula. The m_L mass vanishes at the phase transition point, as was expected from the disappearance of the monopole plasma at the critical temperature. Beyond the phase transition point, the m_T mass measured in this paper does not behave in a physical way due to the severe Gribov copy problem.

Finally, let us comment on the continuum limit of the measured quantities. The continuum limit of $cQED_3$ corresponds to $\beta=1/(g_3^2 a)\to\infty$, holding the dimensionful gauge coupling g_3 fixed. According to Polyakov, nonperturbative quantities such as the Debye mass and string tension can be expressed in terms of g_3 and the monopole density ρ, which generally might be independent quantities. However, this is not true for compact U(1) where both g_3 and ρ depend on a single parameter, the lattice coupling β. Therefore, in the limit of vanishing lattice spacing, the monopole density and other nonperturbative quantities such as the Debye mass, string tension, and anomalous dimension also vanish exponentially as $\sim\exp\{-\text{const}\beta\}$ [cf. Eqs. (67),(69)]. However, in more realistic models (like the Georgi-Glashow model) the monopole density and the lattice spacings are indeed independent and the monopole density should survive in the continuum limit. According to our results, this implies that in the continuum limit of such theories a nonzero anomalous dimension in the photon propagator can be expected.

ACKNOWLEDGMENTS

M.N.Ch. is supported by the JSPS through grant No. P01023. E.-M.I. gratefully appreciates the support by the Ministry of Education, Culture and Science of Japan (Monbu-Kagaku-sho) and the hospitality extended to him by H. Toki at the RCNP of Osaka University.

[1] A. M. Polyakov, Nucl. Phys. **B120**, 429 (1977).
[2] H. R. Fiebig and R. M. Woloshyn, Phys. Rev. D **42**, 3520 (1990).
[3] Y. Hosotani, Phys. Lett. **69B**, 499 (1977); V. K. Onemli, M. Tas, and B. Tekin, J. High Energy Phys. **08**, 046 (2001).
[4] G. Baskaran and P. W. Anderson, Phys. Rev. B **37**, 580 (1998); L. B. Ioffe and A. I. Larkin, *ibid.* **39**, 8988 (1989); P. A. Lee, Phys. Rev. Lett. **63**, 680 (1989); T. R. Morris, Phys. Rev. D **53**, 7250 (1996).
[5] M. N. Chernodub, E.-M. Ilgenfritz, and A. Schiller, Phys. Rev. D **64**, 054507 (2001).
[6] M. N. Chernodub, E.-M. Ilgenfritz, and A. Schiller, Phys. Rev. D **64**, 114502 (2001).
[7] M. N. Chernodub, E.-M. Ilgenfritz, and A. Schiller, Phys. Rev. Lett. **88**, 231601 (2002).
[8] H. Kleinert, F. S. Nogueira, and A. Sudbø, Phys. Rev. Lett. **88**, 232001 (2002); A. Sudbø *et al.*, *ibid.* **89**, 226403 (2002).
[9] M. N. Chernodub, E.-M. Ilgenfritz, and A. Schiller, Phys. Lett. B **547**, 269 (2002).
[10] M. I. Polikarpov, Ken Yee, and M. A. Zubkov, Phys. Rev. D **48**, 3377 (1993).
[11] R. J. Wensley and J. D. Stack, Phys. Rev. Lett. **63**, 1764 (1989).
[12] T. DeGrand and D. Toussaint, Phys. Rev. D **22**, 2478 (1980).
[13] P. H. Damgaard and U. M. Heller, Nucl. Phys. **B309**, 625 (1988).
[14] V. K. Mitrjushkin, Phys. Lett. B **390**, 293 (1997); I. L. Bogolubsky, V. K. Mitrjushkin, M. Müller-Preussker, and P. Peter, *ibid.* **458**, 102 (1999).
[15] P. Marenzoni, G. Martinelli, N. Stella, and M. Testa, Phys. Lett. B **318**, 511 (1993); P. Marenzoni, G. Martinelli, and N. Stella, Nucl. Phys. **B455**, 339 (1995); D. B. Leinweber, J. I. Skullerud, A. G. Williams, and C. Parrinello, Phys. Rev. D **60**, 094507 (1999); **61**, 079901E (1999); A. G. Williams, in Proceedings of the 3rd International Conference on Quark Confinement and the Hadron Spectrum, hep-ph/9809201.
[16] J. P. Ma, Mod. Phys. Lett. A **15**, 229 (2000).
[17] W. Kerler, C. Rebbi, and A. Weber, Phys. Lett. B **348**, 565 (1995).